

Filming non-adiabatic population transfer with x-ray diffraction

Matthew R. Ware,^{1,2} James M. Glowia,³ James P. Cryan,¹
Robert Hartsock,¹ Adi Natan,¹ and Philip H. Bucksbaum^{1,2,4}

¹Stanford PULSE Institute, SLAC National Accelerator Laboratory, Menlo Park, CA 94025, USA

²Department of Physics, Stanford University, Stanford, California 94305, USA*

³LCLS, SLAC National Accelerator Laboratory, Menlo Park, CA 94025, USA

⁴Department of Applied Physics, Stanford University, Stanford, California 94305, USA

(Dated: December 14, 2024)

We show that femtosecond x-ray scattering from molecules prepared in a superposition of electronic states moving through an avoided crossing has new features not found in diffraction from the corresponding classical mixed state. Photoabsorption in molecular iodine at 520 nm produces a coherent superposition of two different dipole-allowed nearly degenerate excited states, which interact due to non-adiabatic coupling. We show that the mixing of the nuclear wavepackets from the two electronic states at the avoided crossing leads to ultrafast changes in the angular composition of the scattering pattern. This provides a novel means to study transitions in excited molecular systems. We reconstruct a movie of the nuclear probability density arising from this interference.

Diffraction with femtosecond pulses from X-ray free-electron lasers (FELs) is a powerful technique to image the geometry and motion of atoms in molecules. It has been used to image vibrational modes and dissociation in molecular gases, clusters, and solutions [1–5]. Here we extend this method to the study of nonadiabatic transitions in molecules.

Within the conventional Born-Oppenheimer Approximation (BOA) used to describe the structure of molecules, electronic motion and nuclear motion are treated separately because of the disparity in their timescales. Nuclear motion has been observed with ultrafast x-ray diffraction. However, electronic motion has yet to be resolved with ultrafast x-ray scattering, because the cross-section for scattering between valence excited states is highly suppressed in large molecular systems [6]. For small atomic systems like hydrogen, simulations have shown that electronic motion may be observed in x-ray diffraction, but the challenge for these systems is preparing a coherent superposition of electronic states with a beat period longer than the x-ray pulse duration [7]. Thus, x-ray scattering is at present a limited probe, able to resolve rovibrational motion on potential energy surfaces, but unable to detect the full rovibronic quantum coherence between BOA potential energy surfaces, even though laser methods have recorded that these coherences can persist for tens of picoseconds in molecular gases [8].

There are several recent proposals to overcome this limitation [7, 9]. Here we demonstrate that ultrafast x-ray diffraction can detect the quantum coherence between electronic states near degeneracies that lead to nonadiabatic population transfer. For diatomic molecules at avoided crossings, these non-adiabatic terms in the Hamiltonian dominate the system evolution [10].

Figure 1 shows a system where such near degeneracies are present and sketches out the non-adiabatic dynamics. Laser-induced resonant photoabsorption in molecu-

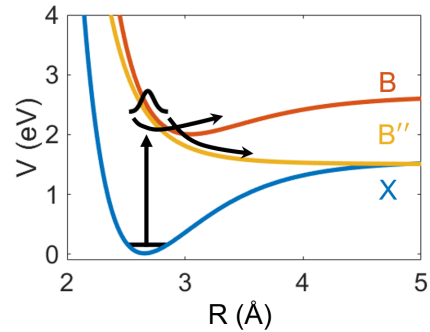


FIG. 1: Potential energy diagram of the electronic states in molecular iodine a single 520 nm photon may access. The X to B transition is a parallel excitation. The X to B'' transition is a perpendicular excitation [15, 16]. The two trajectories highlight the non-adiabatic population transfer near the avoided crossing.

lar iodine from the X ($^1\Sigma_g^+$) state at 520nm produces a superposition of the bound B ($^3\Pi_{0+u}$) state and dissociative B'' ($^1\Pi_u$) state in the ratio 4:1 [11]. The B and B'' states can exchange population through nuclear motion and spin-orbit coupling [12–14]. For example, the initial wavepacket dissociating on the B'' state can be recaptured in the region of the avoided crossing by making a non-adiabatic transition onto the bound B state. This should be seen in x-ray scattering, as we now explain.

The time-dependent x-ray scattering intensity may be expressed as

$$\frac{dI}{d\Omega} = \frac{d\sigma_{Th}}{d\Omega} \int d\vec{k} I(\vec{k}) \frac{\omega}{\omega_s} \langle \psi(\tau) | \hat{F}(\vec{Q}) | \psi(\tau) \rangle \quad (1)$$

where $\frac{d\sigma_{Th}}{d\Omega}$ is the Thomson scattering cross-section, $I(\vec{k})$ is the incident x-ray flux, $|\psi(\tau)\rangle$ is the state of the molecule at pump-probe delay τ , \vec{k} is the incident x-ray momentum, \vec{k}_s is the scattered x-ray momentum,

$\vec{Q} = \vec{k} - \vec{k}_s$ is the momentum transfer, and $\hat{F}(\vec{Q}) = \sum_{j,l} e^{i\vec{Q}\cdot(\vec{r}_j - \vec{r}_l)}$ is the scattering operator, where $\vec{r}_{j,l}$ are the electronic coordinates [17].

For scattering within the pulse bandwidth ($\omega \approx \omega_s$) and collimated x-ray beam input I_0 , this is the product of three factors:

$$\frac{dI}{d\Omega} = \frac{d\sigma_{Th}}{d\Omega} I_0 S(\vec{Q}, \tau) \quad (2)$$

where $S(\vec{Q}, \tau)$ is a time- and angle-dependent Thomson-corrected scattering probability, which arises from the expectation value of the scattering operator \hat{F} in Eqn. 1 with respect to the full molecular wavefunction.

The scattering expression $S_N(\vec{Q}, \tau)$ for each electronic state N is simplified considerably by the independent atom approximation so that the scattering probability for a homonuclear diatomic molecule becomes a simple function of the atomic separation \vec{R} [18]:

$$S_N(\vec{Q}, \tau) = 2 \left| f_A(\vec{Q}) \right|^2 \left(1 + \text{Re} \left\{ \int d\vec{R} \rho_N(\vec{R}, \tau) e^{i\vec{Q}\cdot\vec{R}} \right\} \right). \quad (3)$$

Here $f_A(Q)$ is the atomic scattering factor and $\rho_N(\vec{R}, \tau)$ is the ensemble-averaged nuclear probability density of electronic state N at time τ . The exponential function in Eqn. 3 can be rewritten using the spherical Bessel expansion:

$$e^{i\vec{Q}\cdot\vec{R}} = \sum_l i^l (2l+1) P_l(\cos \theta) j_l(QR). \quad (4)$$

where $j_l(QR)$ is the l th spherical Bessel function. The x-ray diffraction pattern projects onto Legendre polynomials that describe the target probability density [19, 20]. For inversion-symmetric systems, e.g. the nuclear probability density following dipole excitations, only *even* Legendre polynomials contribute:

$$S_N(Q, \theta, \tau) = \sum_{l=0,2,\dots} \sqrt{\frac{2\pi}{2l+1}} P_l(\cos \theta) S_{N,l}(Q, \tau). \quad (5)$$

This analysis suggests that ultrafast transitions between different electronic states can be detected by ultrafast changes in the Legendre decomposition of the scattering pattern. This provides a novel means to study transitions in excited molecular systems. We now apply these ideas to x-ray scattering in molecular iodine.

Prior to photoexcitation, the initial iodine molecular ensemble is a thermal equilibrium distribution of rovibrational states on the ground (X) BOA electronic potential energy surface. It is both isotropic and time-independent, so $S_X(Q)$ is also independent of time and isotropic.

The signal after photoexcitation is neither isotropic nor time-independent. Isotropy is broken because excitation probabilities for the $X \rightarrow B$ and $X \rightarrow B''$ transitions have

an angle dependence of $\cos^2 \theta$ and $\sin^2 \theta$, respectively, where θ is the angle of the interatomic axis with respect to the excitation laser polarization.

The two terms $P_0(\cos \theta) = 1$ and $P_2(\cos \theta) = (3 \cos^2 \theta - 1)/2$ are sufficient to describe the scattering following direct single-photon excitation either to B or B'', whereas the scattering is completely described by the isotropic term P_0 prior to excitation.

The time dependence of the x-ray scattering pattern following excitation is more complicated, but once again the BOA framework simplifies the analysis by treating each electronic state as an independent potential energy surface in the geometrical space of atomic positions. The excitation therefore separates into two wave packets with time-dependent ensemble-averaged nuclear probability densities $\rho_B(\vec{R}, t)$ and $\rho_{B''}(\vec{R}, t)$ on the B and B'' excited state surface, respectively:

$$\begin{aligned} S(Q, \theta, \tau) = & S_X(Q, \theta, \tau) + S_B(Q, \theta, \tau) + S_{B''}(Q, \theta, \tau) = \\ & P_0(\cos \theta) [S_{X,0}(Q, \tau) + S_{B,0}(Q, \tau) + S_{B'',0}(Q, \tau)] + \\ & P_2(\cos \theta) [S_{B,2}(Q, \tau) + S_{B'',2}(Q, \tau)]. \end{aligned} \quad (6)$$

The $l = 0$ and $l = 2$ terms in Eqn. 5 thus describe the angular dependence of this scattered x-ray intensity distribution.

Wave packets excited from X to the B and B'' states pass through an avoided crossing within the first 40-60 fs [12], when the iodine atoms are separated by about 3 Å as shown in Fig. 1. Non-adiabatic transitions at this point can transfer population from B to B'', or vice versa. For example, this could increase the fraction of dissociating molecules, which increases $S_{B''}(\vec{Q}, \tau)$ and decreases $S_B(\vec{Q}, \tau)$. Since these scattering patterns evolve in distinct ways, this change is observable. The Legendre decomposition coefficients in Eqn. 5 will change as well, but for a classical mixture of molecules in the B or B'' state the scattering is still always confined to Legendre components with $l = 0$ and 2.

It is more proper to consider the electronic excitation as 2-component quantum superposition state $|a \cos \theta \psi_B + b \sin \theta \psi_{B''}\rangle$. For nondegenerate B and B'' the complex coefficients a and b evolve rapidly in phase, and this has led previous analyses to conclude that the scattering behavior is identical to a classical mixture [6]. However, from the Franck-Condon point to the avoided crossing, the B and B'' states are nearly degenerate, so the scattering acquires an additional term due to the non-adiabatic coupling between the states:

$$\begin{aligned} \langle \hat{H}' \rangle = & \begin{pmatrix} a \cos \theta & b \sin \theta \end{pmatrix} \begin{pmatrix} 0 & H' \\ H'^* & 0 \end{pmatrix} \begin{pmatrix} a \cos \theta \\ b \sin \theta \end{pmatrix} \quad (7) \\ & \propto \cos \theta \sin \theta \end{aligned}$$

In lowest order (the Landau-Zener approximation) this contributes a term proportional to $\cos^2 \theta \sin^2 \theta$ to the

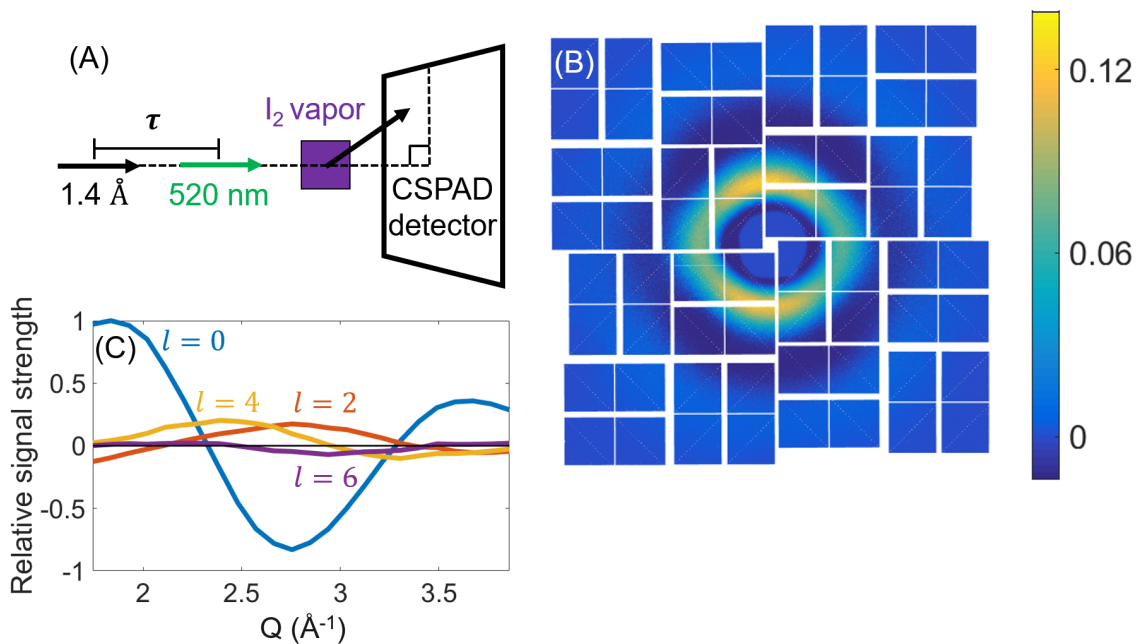


FIG. 2: (A) Beamline schematic in the XPP hutch at the LCLS. (B) A representative image of the Thomson-corrected x-ray scattering signal at the detector for an optical-pump-x-ray-probe delay of 120 fs with the early-time average subtracted using five x-ray pulses from the LCLS. The scale is in arbitrary detector units relative to the maximum of $S(\vec{Q}, \tau)$ at this delay. The data are scaled at each radius in Q to account for the normalization over the Ewalds sphere, $Q^2 (S(\vec{Q}, \tau) - \bar{S}(\vec{Q}, \tau < 0))$. (C) We show the projection of the CSPAD image onto the zeroth, second, fourth, and sixth order Legendre polynomials as described in Eqn. 5 in the text.

scattering, which can be decomposed into Legendre terms with $l = 0, 2, 4$. More generally the evolution of a coherent preparation described by $\rho(\vec{R}, \tau)$ under this Hamiltonian should lead to additional even orders of $P_l(\cos \theta)$ higher than $l = 2$.

This was tested using data from a 2016 LCLS experiment on molecular iodine vapor resonantly excited from the X state to the B and B' states by an ultrafast laser (520 ± 5 nm, $40 \mu\text{J}$, 50fs, vertically polarized, focused to $\sim 10^{12}$ W/cm²), and probed by a spatially coherent beam of 9.0 keV 2 mJ 40 fs horizontally polarized x-rays provided by the LCLS [2]. The copropagating cross-polarized visible and x-ray laser beams were focused into molecular iodine vapor with a column density of $\sim 10^{18}$ cm⁻². Approximately 10^7 x-rays per pulse were scattered onto a 2.3 megapixel silicon array (CSPAD) [21]. Figure 2 shows a representative image of the signal at the detector. Up to 50 scattered x-rays per pulse per pixel were detected. The x-rays probe the iodine at a variable time delay following photoexcitation, producing an x-ray scattering signal $dI(Q, \theta, \tau)/d\Omega$ as described by Eqn. 2.

The Legendre decomposition analysis of Eqn. 5 is shown in Figure 3. The mean values of patterns before $\tau = 0$ have been subtracted to remove S_X as well as the detector imperfections. In addition to the strong expected contributions to scattering from $l = 0$ and $l = 2$,

we see clear contributions from $l = 4$, and in addition to this there is a smaller but still distinct contribution for $l = 6$.

We have verified this signal is physical and not a detector artifact or issue with projecting the data. The $l > 2$ signal disappears if we change the wavelength to 800nm, and the signal strength is reduced by 1/4 if we use elliptically polarized light instead of linearly polarized light. Moreover, each Legendre order of the data in Figure 3 has an associated phase shift consistent with the associated spherical Bessel functions at low Q from Eqn. 4.

The selection rules for single-photon excitation cannot account for $l \geq 4$, suggesting some additional interaction. There are two candidates: (1) Higher order (multiphoton or Raman) terms left out of the photoexcitation description lead to higher powers of $\cos \theta$ and $\sin \theta$ in $\rho(\vec{R}, t)$. Or (2) the coupling shown in Eqn. 7 leads to cross-terms that project onto all even orders of Legendre polynomials.

(1) In the case of multiphoton excitations, we would anticipate the ensemble to have an initial distribution like $\cos^{2n} \theta \sin^{2m} \theta$ at t_0 , which would project at most onto $P_{2n+2m}(\cos \theta)$ at t_0 and the subsequent dephasing would decrease the order of this projection.

(2) In the case of the non-radiative coupling described

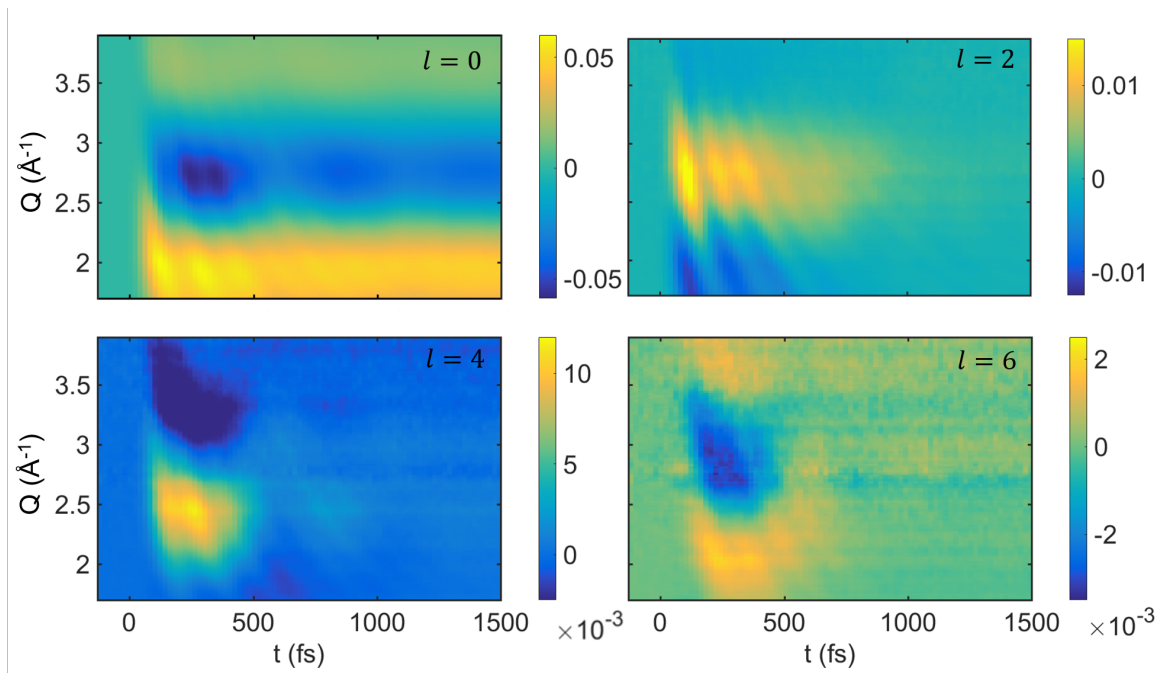


FIG. 3: Thomson-corrected difference signal $\Delta S_l(Q, \tau) = S_l(Q, \tau) - \bar{S}_l(Q, \tau < 0)$ projections onto Legendre polynomials, $P_l(\cos \theta)$ for $l = 0$, $l = 2$, $l = 4$, and $l = 6$. (See Eqn. 5). The $l = 0$ and $l = 2$ projections are expected from classical considerations, but the $l = 4$ and $l = 6$ projections are evidence for wave packets in a quantum superposition of B and B''. The signal in $l \geq 2$ decay due to rotational dephasing [2]. Each projection has a relative phase shift due to the spherical Bessel transformation it is associated with. We have scaled the figures relative to the maximum signal strength in $S_0(Q, \tau)$. The sign change from $l = 4$ to $l = 6$ and the relative peak signal strengths of $l = 4$ and $l = 6$ are both consistent with the Legendre expansion of $\cos \theta \sin \theta$ from Eqn. 7.

in Eqn. 7, the x-ray diffraction would only project onto $l = 0$ and 2 at the time of excitation. Following mixing of the wavepackets due to the avoided crossing, the system can project onto $l \geq 4$.

The higher order Legendre components of the scattering data have two distinctive features that help us to understand their origin:

- The real-space reconstruction of the $l = 4$ and $l = 6$ Legendre projections unveil dynamics consistent with the B and B'' states. We show the $l = 4$ reconstruction in Fig. 4. To recover the real-space dynamics, we invert the associated spherical Bessel transformations from Eqn. 5. (For diatomics, the inverse spherical Bessel transformation reconstructs the nuclear charge density. For molecules with more than two atoms, the transformation produces the pair-correlation functions [20].) We identify the bound B state by its period of $T = 550$ fs about an equilibrium position of 3 Å, and we identify the dissociation on the B'' state by the dissociation velocity of 18.6 ± 2.2 Å/ps, consistent with the dissociation velocity estimate of 16.7 Å/ps from the kinetic energy release. We therefore see no indication of (1) Raman excitation on the ground state nor higher lying electronic states above the B states. We do see a clear indication that (2) the B and B'' states are responsible for the time-delayed $l \geq 4$

signal.

- The integrated signal of each term is delayed by 50 ± 20 fs with respect to the zeroth and second order Legendre projections Figure 5. This delayed response is consistent with (2) the 40-60 fs that the wavepackets take to pass through the avoided crossing, and also appears in the delayed onset of the oscillating wave packet in Fig. 4.

We conclude that the $l \geq 4$ scattering distributions result from the interference of the B and B'' wavepackets following mixing at the avoided crossing. After population transfer onto the B state through spin-orbit coupling, the initially dissociative state becomes bound. Likewise, some of the initial B state population transfers to the dissociative B'' state.

In summary, we have observed the transfer of population between coherently prepared B and B'' wave packets in iodine as they pass through an avoided crossing and have reconstructed the subsequent dynamics arising from their quantum interference. We see the coherent interference on both the bound B state and the dissociative B'' state through the time-delayed, higher order Legendre projections of the x-ray diffraction. This also demonstrates that the same mechanism which leads to predissociation of a bound state also leads to preassocia-

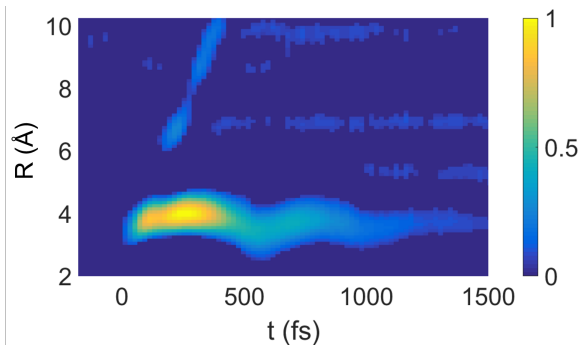


FIG. 4: Real-space reconstruction of the Legendre 4 projection of the x-ray diffraction data. Legendre 6 produces the same features with reduced fidelity. We observe a dissociation along the B'' state of velocity $18.6 \pm 2.2 \text{ \AA/ps}$ and periodic bound state motion ($T=550 \text{ fs}$) within the B state. The vibrational motion clearly shows the delayed onset, appearing at 3 \AA , 50 fs after the excitation. The dissociation signal from $4.5 - 6 \text{ \AA}$ at 100 fs disappears due to the limited Q range of the experiment, and the horizontal lines are artifacts of the reconstruction due to the limited Q range.

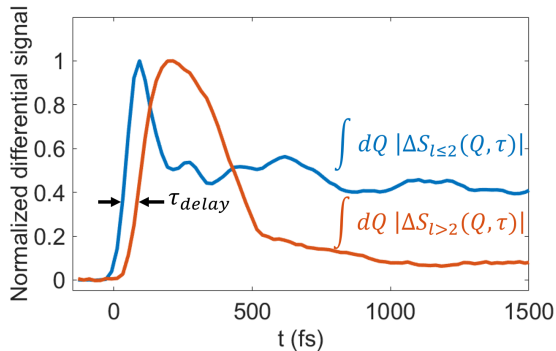


FIG. 5: The higher order Legendre projections are delayed by $\tau_{\text{delay}} = 50 \pm 20 \text{ fs}$. This signal is consistent with evolution via non-adiabatic and spin-orbit coupling at the avoided crossing.

tion, i.e. preemptive capture of a dissociating molecule.

Moreover, while directly resolving electronic motion through inelastic x-ray scattering is an outstanding experimental challenge, this paper demonstrates that the coherence between electronic states can be observed using time-resolved x-ray scattering. Near avoided crossing and even conical intersections, the mixing of nuclear wave-packets of different symmetries will in general lead to an ultrafast change in the symmetry of the x-ray scattering.

We wish to acknowledge the Glowntia L2816 collaboration for access to data from their LCLS experiment, which were used in this analysis, and we wish to acknowledge useful discussions with Tais Gorkhover in the prepa-

ration of this letter. This research is supported through the Stanford PULSE Institute, SLAC National Accelerator Laboratory by the U.S. Department of Energy, Office of Basic Energy Sciences, Atomic, Molecular, and Optical Science Program. Use of the Linac Coherent Light Source (LCLS), SLAC National Accelerator Laboratory, is supported by the U.S. Department of Energy, Office of Basic Energy Sciences under Contract No. DE-AC02-76SF00515. Matthew Ware is supported by the Stanford Graduate Fellowship.

* mrware@stanford.edu

- [1] M. Minitti, J. Budarz, A. Kirrander, J. Robinson, D. Ratner, T. Lane, D. Zhu, J. Glowntia, M. Kozina, H. Lemke, M. Sikorski, Y. Feng, S. Nelson, K. Saita, B. Stankus, T. Northey, J. Hastings, and P. Weber, *Physical Review Letters* **114**, 255501 (2015).
- [2] J. Glowntia, A. Natan, J. Cryan, R. Hartsock, M. Kozina, M. Minitti, S. Nelson, J. Robinson, T. Sato, T. van Driel, G. Welch, C. Weninger, D. Zhu, and P. Bucksbaum, *Physical Review Letters* **117**, 153003 (2016).
- [3] J. Kupper, S. Stern, L. Holmegaard, F. Filsinger, A. Rouze, A. Rudenko, P. Johnsson, A. V. Martin, M. Adolph, A. Aquila, S. Bajt, A. Barty, C. Bostedt, J. Bozek, C. Caleman, R. Coffee, N. Coppola, T. Delmas, S. Epp, B. Erk, L. Foucar, T. Gorkhover, L. Gumprecht, A. Hartmann, R. Hartmann, G. Hauser, P. Holl, A. Hmke, N. Kimmel, F. Krasniqi, K.-U. Khnel, J. Maurer, M. Messerschmidt, R. Moshhammer, C. Reich, B. Rudek, R. Santra, I. Schlichting, C. Schmidt, S. Schorb, J. Schulz, H. Soltau, J. C. Spence, D. Starodub, L. Strder, J. Thgersen, M. J. Vrakking, G. Weidenspointner, T. A. White, C. Wunderer, G. Meijer, J. Ullrich, H. Stapelfeldt, D. Rolles, and H. N. Chapman, *Physical Review Letters* **112**, 083002 (2014).
- [4] T. Gorkhover, M. Adolph, D. Rupp, S. Schorb, S. W. Epp, B. Erk, L. Foucar, R. Hartmann, N. Kimmel, K.-U. Kühnel, D. Rolles, B. Rudek, A. Rudenko, R. Andritschke, A. Aquila, J. D. Bozek, N. Coppola, T. Erke, F. Filsinger, H. Gorke, H. Graafsmma, L. Gumprecht, G. Hauser, S. Herrmann, H. Hirsemann, A. Hömke, P. Holl, C. Kaiser, F. Krasniqi, J.-H. Meyer, M. Matysek, M. Messerschmidt, D. Miessner, B. Nilsson, D. Pietschner, G. Potdevin, C. Reich, G. Schaller, C. Schmidt, F. Schopper, C. D. Schröter, J. Schulz, H. Soltau, G. Weidenspointner, I. Schlichting, L. Strüder, J. Ullrich, T. Möller, and C. Bostedt, *Phys. Rev. Lett.* **108**, 245005 (2012).
- [5] T. B. Van Driel, K. S. Kjær, R. W. Hartsock, A. O. Dohn, T. Harlang, M. Chollet, M. Christensen, W. Gawelda, N. E. Henriksen, J. G. Kim, *et al.*, *Nature communications* **7**, 13678 (2016).
- [6] K. Bennett, M. Kowalewski, and S. Mukamel, arXiv:1611.07085 [physics] (2016), arXiv: 1611.07085.
- [7] G. Dixit, O. Vendrell, and R. Santra, *Proceedings of the National Academy of Sciences* **109**, 11636 (2012).
- [8] M. Comstock, V. V. Lozovoy, and M. Dantus, *The Journal of Chemical Physics* **119**, 65466553 (2003).
- [9] M. Kowalewski, K. Bennett, and S. Mukamel,

- Structural Dynamics **4**, 054101 (2017), <http://dx.doi.org/10.1063/1.4984241>.
- [10] C. Liekhus-Schmaltz, G. A. McCracken, A. Kaldun, J. P. Cryan, and P. H. Bucksbaum, *The Journal of Chemical Physics* **145**, 144304 (2016).
- [11] J. Tellinghuisen, *The Journal of Chemical Physics* **76**, 4736 (1982).
- [12] N. F. Scherer, L. D. Ziegler, and G. R. Fleming, *The Journal of Chemical Physics* **96**, 5544 (1992).
- [13] M. Broyer, J.-C. Lehmann, and J. Vigue, *Journal de Physique* **36**, 235 (1975).
- [14] M. Broyer, J. Vigue, and J. C. Lehmann, *The Journal of Chemical Physics* **63**, 5428 (1975).
- [15] J. Tellinghuisen, *The Journal of Chemical Physics* **57**, 2397 (1972).
- [16] R. S. Mulliken, *The Journal of Chemical Physics* **55**, 288 (1971).
- [17] S. Hau-Riege, “X-ray scattering,” in *Nonrelativistic Quantum X-Ray Physics* (Wiley-VCH Verlag, 2014) pp. 235–264.
- [18] N. E. Henriksen and K. B. Moller, *The Journal of Physical Chemistry B* **112**, 558 (2008).
- [19] J. S. Baskin and A. H. Zewail, *ChemPhysChem* **7**, 1562 (2006).
- [20] U. Lorenz, K. B. Moller, and N. E. Henriksen, *New Journal of Physics* **12**, 113022 (2010).
- [21] G. Blaj, P. Caragiulo, G. Carini, S. Carron, A. Dragone, D. Freytag, G. Haller, P. Hart, J. Hasi, R. Herbst, S. Herrmann, C. Kenney, B. Markovic, K. Nishimura, S. Osier, J. Pines, B. Reese, J. Segal, A. Tomada, and M. Weaver, *Journal of Synchrotron Radiation* **22**, 577 (2015).